Understanding the electronic structure and magnetism of correlated nanosystems

2009 J. Phys.: Condens. Matter 21 064248

(http://iopscience.iop.org/0953-8984/21/6/064248)

IOP Publishing Journal of Physics: Condensed Matter

J. Phys.: Condens. Matter **21** (2009) 064248 (7pp) doi:10.1088/0953-8984/21/6/064248

Understanding the electronic structure and magnetism of correlated nanosystems

H Hafermann[1], S Brener[1], A N Rubtsov[2], M I Katsnelson[3] and A I Lichtenstein[1]

[1] I. Institute of Theoretical Physics, University of Hamburg, D-20355 Hamburg, Germany
[2] Department of Physics, Moscow State University, 119992 Moscow, Russia
[3] Institute for Molecules and Materials, Radboud University of Nijmegen, 6525 AJ Nijmegen, The Netherlands

E-mail: hartmut.hafermann@physnet.uni-hamburg.de

Received 8 August 2008
Published 20 January 2009
Online at stacks.iop.org/JPhysCM/21/064248

Abstract

In this paper we review recent developments towards a realistic description of the electronic structure and magnetism of correlated nanosystems. A new class of so-called continuous-time solvers for the quantum impurity problem is discussed, which provides a numerically exact solution without systematic errors due to imaginary time discretization. These solvers are able to handle general interactions, like the full Coulomb vertex. We further show how four-point or higher-order correlation functions of the impurity problem can be computed. This allows the calculation of dynamical susceptibilities which provide information about spin excitations. Moreover, we discuss a principally new many-body scheme recently proposed for the description of non-local correlations in strongly correlated systems. This approach provides a basis for a many-body description of extended correlated nanostructures on a substrate.

(Some figures in this article are in colour only in the electronic version)

1. Introduction

Understanding correlated nanosystems is at the heart of modern condensed matter physics. Advances in experimental techniques have rendered it possible to manipulate, control and investigate matter on the nanoscale. This has opened up a whole new world of opportunities and raised new questions concerning the role of many-body effects in geometrically constrained systems.

Nowadays, nanostructures are almost routinely assembled by moving individual atoms on a surface with atomic precision [1] or through processes of self-organization [2]. Scanning tunneling microscopy allows us not only to manipulate, but also to directly probe, the magnetism and spectral properties of nanosystems on metallic or semimetallic substrates. Spin excitation spectra and collective modes can be probed by inelastic tunneling spectroscopy [3], and recently even the hysteresis of individual atoms was observed [4].

An important issue in understanding nanosystems is the effect of the correlations. These are usually enhanced due to the reduced dimensionality. The interplay between spin and charge degrees of freedom in conjunction with the many-body character of a system can give rise to new exotic ground states or induce low energy many-body resonances, like the Kondo effect [5]. The interaction of magnetic adatoms with a metallic surface or magnetic interactions between atoms can significantly alter the spectral properties of a nanosystem [6]. Furthermore, the spectral properties turn out to be sensitive to geometry [7, 8].

A further topic of fundamental research is the evolution of magnetism from single atoms to extended nanostructures such as islands [9] and chains [10, 11] on surfaces. In low-dimensional systems fluctuations become important and long-range order at finite temperature is prohibited in truly one- or two-dimensional systems by the Mermin–Wagner theorem [12]. Nevertheless, it has been demonstrated that Co atoms on a Pt surface indeed exhibit ferromagnetism below a critical temperature [13]. The question remains how the interplay of anisotropies, interaction with the substrate and correlations result in an ordered state and clearly requires a realistic description of the system as a whole.

Another nontrivial aspect is the material dependence. The framework of density functional theory (DFT) provides

a quantitative description of many materials. While providing predictive power for properties such as equilibrium positions [2] or exchange interactions [14], the failure of approximations to the DFT, such as the local density approximation (LDA), to capture the physics of strong correlations renders a realistic description of correlated low-dimensional nanosystems difficult. On the other hand, many-body approaches for the correlated system usually employ simple model Hamiltonians to describe the effect of the correlations and hence can overlook a nontrivial material dependence. In order to develop a material-specific theory of magnetism of correlated nanosystems, methods are needed to combine the *ab initio* with many-body approaches. A successful route to incorporate the material aspect into many-body computations is the combination of the dynamical mean-field theory (DMFT) with the local density approximation, the so-called LDA + DMFT approach [15]. The DMFT maps the lattice problem onto an effective local multiorbital quantum impurity problem subject to a self-consistency condition for the impurity-bath hybridization function. The material dependence as described by the corresponding LDA Hamiltonian enters here. Magnetic adatoms on a metallic surface can also be described in terms of an impurity model in which the hybridization with the host material contains the material-specific features. However, the solution of the underlying multiorbital quantum impurity problem still remains a formidable task. Quantum Monte Carlo methods are used as a standard tool for this purpose. A well-known type of solver is the Hirsch–Fye algorithm [16]. It is based on a discretization of the imaginary time interval into time slices and a Trotter breakup of the partition function. A Hubbard–Stratonovich transformation is used to decouple the fermionic degrees of freedom, which introduces an auxiliary field on each of the time slices. The algorithm samples all configurations of the auxiliary field. This approach has two major drawbacks: the time discretization introduces systematic errors and the scheme lacks decouplings for general types of interaction.

In the next section we will discuss two complementary approaches to solve the quantum impurity problem that overcome these problems [17–19]: these build on an expansion of the imaginary time partition function in either the interaction (weak coupling approach) or the impurity-bath hybridization (strong coupling expansion) and the collection of diagrams into fermionic determinants. These algorithms provide a numerically exact solution of the problem, without any systematic errors and can treat general interactions.

These techniques are the key tools for solving a single multiorbital impurity problem. The calculation of the properties of a collection of such impurities is, however, not computationally feasible due to the exponential growth of the Hilbert space. In order to tackle problems such as long-range order or magnetism in extended nanostructures, different approaches are required. Recently, a novel diagrammatic expansion around the DMFT has been proposed in the context of lattice problems [20]. This so-called dual fermion approach allows us to incorporate spatial correlations into calculations of strongly correlated systems. We will give a formulation suitable for a realistic treatment of extended nanostructures exerted to the influence of a substrate. We further discuss the extension of this approach to the calculation of the two-particle Green function which gives access to, for example, magnetic instabilities of correlated systems [21].

2. Numerically exact solvers for the quantum impurity problem

In this section we contrast the weak and strong coupling continuous-time algorithms for solving the impurity problem. For notational convenience, we consider the case of a single-band Hubbard impurity in a bath described by the time-dependent hybridization function Δ. The imaginary time action for this particular case is given by

$$S = \sum_\sigma \int_0^\beta \mathrm{d}\tau \int_0^\beta \mathrm{d}\tau'\, c_\sigma^*(\tau)[\partial_\tau - \mu + \Delta(\tau-\tau')]c_\sigma(\tau') + U\int_0^\beta \mathrm{d}\tau\, c_\uparrow^*(\tau)c_\uparrow(\tau)c_\downarrow^*(\tau)c_\downarrow(\tau). \tag{1}$$

Let us consider the weak coupling case first. A generalization of the weak coupling algorithm to the multiorbital case and for general non-local in time interactions can be found in [17]. Up to an irrelevant multiplicative constant, we can divide the action into a Gaussian part S_0 and an interaction part as follows:

$$S_0 = \sum_\sigma \int_0^\beta \mathrm{d}\tau \int_0^\beta \mathrm{d}\tau'\, c_\sigma^*(\tau)[\partial_\tau - \mu + \Delta(\tau-\tau') + U\alpha_{-\sigma}\delta(\tau-\tau')]c_\sigma(\tau'), \tag{2}$$

$$S_U = U\int_0^\beta \mathrm{d}\tau\, (c_\uparrow^*(\tau)c_\uparrow(\tau) - \alpha_\uparrow(\tau))(c_\downarrow^*(\tau)c_\downarrow(\tau) - \alpha_\downarrow(\tau)). \tag{3}$$

The introduction of the so-called α parameters will be to control the sign problem, as discussed below. Defining the average over the noninteracting system as $\langle\cdots\rangle_0 = (1/\mathcal{Z}_0)\int\cdots\exp(-S_0)\mathcal{D}[c^*,c]$, the partition function $\mathcal{Z} = \int\exp(-S)\mathcal{D}[c^*,c]$ may now be written in terms of a formal series expansion of the exponential in the interaction term:

$$\mathcal{Z} = \sum_{k=0}^\infty \sum_{\sigma_1}\int_0^\beta \mathrm{d}\tau_1 \cdots \sum_{\sigma_k}\int_0^\beta \mathrm{d}\tau_k\, \mathrm{sgn}(\Omega_k)\,|\Omega_k| \tag{4}$$

where

$$\Omega_k = \frac{(-1)^k}{k!}U^k\langle(c_{\sigma_1}^*c_{\sigma_1} - \alpha_{\sigma_1})(c_{-\sigma_1}^*c_{-\sigma_1} - \alpha_{-\sigma_1})\cdots \cdots(c_{\sigma_k}^*c_{\sigma_k} - \alpha_{\sigma_k})(c_{-\sigma_k}^*c_{-\sigma_k} - \alpha_{-\sigma_k})\rangle_0. \tag{5}$$

Since S_0 is Gaussian, Wick's theorem is applicable and the above noninteracting average may be expressed as a determinant of Green's functions of the noninteracting system, $\Omega_k \sim \prod_\sigma \det\parallel \hat{G}_{ij\sigma}\parallel$, $\hat{G}_{ij\sigma} = G_{0\sigma}(\tau_i - \tau_j) - \alpha_\sigma\delta_{ij}$. A similar expansion can be written for Green's function:

$$G_\sigma(\tau-\tau') = \langle c_\sigma^*(\tau)c_\sigma(\tau')\rangle = \sum_{k=0}^\infty\sum_{\sigma_1}\int_0^\beta \mathrm{d}\tau_1\cdots\sum_{\sigma_k}\int_0^\beta \mathrm{d}\tau_k \times g_\sigma(\tau,\tau';\tau_1,\ldots,\tau_k|\sigma_1,\ldots,\sigma_k)\,\mathrm{sgn}(\Omega_k)\,|\Omega_k| \tag{6}$$

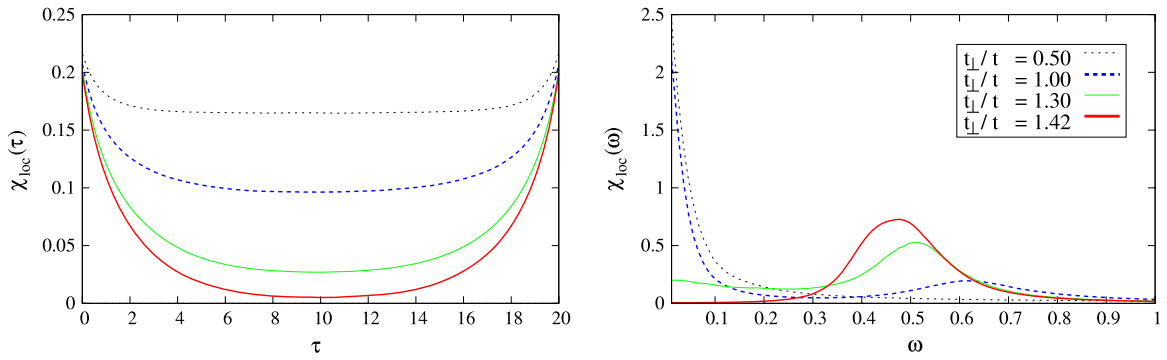

Figure 1. Left: imaginary time correlation function $\chi_{\rm loc}(\tau) = \langle S_z(\tau)S_z(0)\rangle$ for the two-plane Hubbard model on the Bethe lattice. Right: corresponding dynamical susceptibility $\chi_{\rm loc}(\omega)$ obtained by analytical continuation of the imaginary time data [22]. $t_\perp$ denotes the coupling between the two planes. For small $t_\perp$ the two planes couple antiferromagnetically. For $t_\perp > \sqrt{2}$ a singlet between opposing sites on the two planes is formed, accompanied by the development of a spin gap in the dynamical susceptibility [23].

where g is a contribution to Green's function which can be expressed as a ratio of fermionic determinants. The algorithm samples all possible configurations $C_k = \{\tau_1, \ldots, \tau_k|\sigma, \ldots, \sigma_k\}$ of the system by a Markovian random walk according to the probability distribution $|\Omega_k|$. A complication arises in sampling equation (4) since Ω_k is not positive definite: the stronger the sign fluctuates, an increasingly large number of samples is required to acquire proper statistics which may render the simulation unfeasible. However, it can be shown that, for the interaction considered, the 'trivial' sign problem introduced by the factor $(-1)^k$ is completely suppressed by the choice $\alpha_\uparrow = 1 - \alpha_\downarrow$. Other choices for the α's exist for more general interactions. An important point is further to group diagrams with different signs into the determinant. Sampling individual diagrams would also result in a severe sign problem.

By evaluation of the ratio of determinants of matrices of sizes k and $k \pm 1$, it can be shown that the contributions to Green's function for a certain configuration can be obtained as

$$g_\sigma(\tau, \tau'; C_k) = G_{0\sigma}(\tau - \tau') - \sum_{ij=1}^{k} G_{0\sigma}(\tau - \tau_i)\hat{G}^{-1}_{ij\,\sigma} G_{0\sigma}(\tau_j - \tau'), \tag{7}$$

where the elements of the matrix $\hat{G}_{ij}$ contain the noninteracting Green's functions evaluated at the times corresponding to the particular configuration. The Fourier transform of this equation is given by

$$g_\sigma(\omega, \omega'; C_k) = G_{0\sigma}(\omega)\delta_{\omega,\omega'} - \frac{1}{\beta} G_{0\sigma}(\omega)G_{0\sigma}(\omega') \sum_{ij=1}^{k} \mathrm{e}^{\mathrm{i}\omega\tau_i} \hat{G}^{-1}_{ij\,\sigma} \mathrm{e}^{-\mathrm{i}\omega'\tau_j}, \tag{8}$$

and allows us to sample the Green function directly on Matsubara frequencies. Since the algorithm is based on an expansion in the interaction, the contributions to Green's function appear as a correction to a known function (G_0). The Green functions obtained as the Monte Carlo (MC) average $G(\tau - \tau') = \langle g(\tau, \tau'; C_k)\rangle_{\rm MC}$ depend only on the time difference, while the quantities $g(\tau, \tau'; C_k)$ generally do not. In analogy to Wick's theorem, one may construct the corresponding contributions to higher-order correlators. For example, the spin–spin susceptibility $\langle S_z(\tau)S_z(0)\rangle$ with $S_z = (n_\uparrow - n_\downarrow)/2$ can be expressed in terms of the averages $\langle n_\sigma(\tau)n_{\sigma'}(0)\rangle = \langle c^*_\sigma(\tau)c_\sigma(\tau)c^*_{\sigma'}(0)c_{\sigma'}(0)\rangle$. The explicit expression for contributions to this average, which can be obtained by evaluating the determinant ratio for matrices of size k and $k \pm 2$, is given by

$$g_\sigma(\tau, \tau; C_k)g_{\sigma'}(0, 0; C_k) - \delta_{\sigma\sigma'}g_\sigma(\tau, 0; C_k)g_\sigma(0, \tau; C_k), \tag{9}$$

and similar for other averages.

This allows the direct measurement of two-particle functions in imaginary time and subsequent analytical continuation to real frequencies, providing information about two-particle (spin) excitations. As an example, we present results for the two-plane Hubbard model on the Bethe lattice in figure 1. The 'instantaneous' correlators, such as the double occupancy $D = \lim_{\tau\to 0^+}\langle n_\uparrow(\tau)n_\downarrow(0)\rangle$, can be accurately obtained by numerical extrapolation of the limit. The two-particle Green function $\chi^{\sigma\sigma'}_{\omega\omega'\Omega} = \langle c^*_{\sigma\omega+\Omega}c_{\sigma\omega}c^*_{\sigma'\omega'}c_{\sigma'\omega'+\Omega}\rangle$ can be directly measured in the frequency domain using

$$g_\sigma(\omega + \Omega, \omega; C_k)g_{\sigma'}(\omega', \omega' + \Omega; C_k) - \delta_{\sigma\sigma'}g_\sigma(\omega + \Omega, \omega' + \Omega; C_k)g_\sigma(\omega', \omega; C_k). \tag{10}$$

Let us now consider the algorithm based on the strong coupling expansion. We discuss the formalism for the action equation (1). The action is regrouped into the atomic part

$$S_{\rm at} = \sum_\sigma \int_0^\beta \mathrm{d}\tau \int_0^\beta \mathrm{d}\tau'\, c^*_\sigma(\tau)[\partial_\tau - \mu]c_\sigma(\tau') + U\int_0^\beta \mathrm{d}\tau\, c^*_\uparrow(\tau)c_\uparrow(\tau)c^*_\downarrow(\tau)c_\downarrow(\tau) \tag{11}$$

and the part of the action S_Δ which contains the hybridization term. Now a series expansion for the partition function is generated by expanding the exponential in the impurity-bath hybridization (we omit spin indices to simplify the notation):

$$\mathcal{Z} = \int \mathrm{e}^{-S_{\rm at}} \sum_{k=0}^{\infty} \frac{1}{k!} \int_0^\beta \mathrm{d}\tau_1 \int_0^\beta \mathrm{d}\tau_1' \cdots \int_0^\beta \mathrm{d}\tau_k \int_0^\beta \mathrm{d}\tau_k' \times c(\tau_1')c^*(\tau_1)\cdots c(\tau_k')c^*(\tau_k)\Delta(\tau_1 - \tau_1')\cdots\Delta(\tau_k - \tau_k') \times \mathcal{D}[c^*, c]. \tag{12}$$

Here the factor $(-1)^k$ is canceled out by reversing the order of the c and c^* in equation (1). The important observation is that also in this case the functions Δ can be grouped into a determinant. Starting with the time-ordered sequence of times $\tau_k > \cdots > \tau_1$ corresponds to the integrand in equation (12). Then there will be a contribution which stems from the same set of times, but with times τ_k and τ_{k-1} exchanged:

$$c(\tau_1')c^*(\tau_1)\cdots c(\tau_{k-1}')c^*(\tau_k)c(\tau_k')c^*(\tau_{k-1}) \times \Delta(\tau_1-\tau_1')\cdots\Delta(\tau_k-\tau_{k-1}')\Delta(\tau_{k-1}-\tau_k'). \quad (13)$$

Upon time ordering this becomes

$$-c(\tau_1')c^*(\tau_1)\cdots c(\tau_{k-1}')c^*(\tau_{k-1})c(\tau_k')c^*(\tau_k) \times \Delta(\tau_1-\tau_1')\cdots\Delta(\tau_{k-1}-\tau_k')\Delta(\tau_k-\tau_{k-1}'). \quad (14)$$

The $k!$ possible time orderings of the sequence hence yields terms which contain the product of hybridizations, with the times τ_i correspondingly permuted. Since each term appears with the corresponding sign of the permutation, these contributions can be grouped into a determinant:

$$\mathcal{Z} = \mathcal{Z}_{\rm at}\sum_{k=0}^{\infty}\int_0^\beta \mathrm{d}\tau_1\int_{\tau_1}^\beta \mathrm{d}\tau_1'\cdots\int_{\tau_{k-1}'}^\beta \mathrm{d}\tau_k\int_{\tau_k}^\beta \mathrm{d}\tau_k' \times\langle c(\tau_1')c^*(\tau_1)\cdots c(\tau_k')c^*(\tau_k)\rangle_{\rm at} \times \det\parallel\Delta(\tau_i-\tau_j')\parallel. \quad (15)$$

Here $\langle\cdots\rangle_{\rm at} = (1/\mathcal{Z}_{\rm at})\int\cdots\exp(-S_{\rm at})\mathcal{D}[c^*,c]$ denotes the average over the impurity states, which can be computed by exact diagonalization. The explicit time ordering in equation (15) implies that a configuration may be viewed as a collection of segments on the imaginary time interval from 0 to β for each spin. The algorithm samples all possible configurations of these segments. The weight of a configuration is proportional to $\exp(-\delta\tau U)$, where $\delta\tau$ is the overlap between segments for opposite spins. This accounts for the Coulomb repulsion in case the site is doubly occupied.

The measurement of the Green functions has a similar structure as in the weak coupling case. The measurements can be performed in the time or frequency domain and are given by

$$G_\sigma(\tau) = \left\langle\sum_{ij=1}^{k}\hat{\Delta}^{-1}_{ij\sigma}\delta(\tau,\tau_i-\tau_j)\right\rangle_{\rm MC}$$
$$G_\sigma(\omega) = \frac{1}{\beta}\left\langle\sum_{ij=1}^{k}\hat{\Delta}^{-1}_{ij\sigma}\mathrm{e}^{\mathrm{i}\omega(\tau_i-\tau_j)}\right\rangle_{\rm MC} \quad (16)$$

where $\hat{\Delta}$ is the matrix of hybridizations. A few notes on the two approaches are in place: although the methods expand around different limits, the algorithms are numerically exact: in principle, *all* diagrams of a given problem are sampled and hence both approaches will eventually converge to the same result. The average perturbation order $\langle k\rangle_{\rm MC}$, which determines the average size of the matrices which need to be updated in every MC step, however, will be different for the same problem. For the weak coupling solver the perturbation order grows as U is increased, while in the strong coupling case it increases with increasing hybridization strength. Hence the two algorithms will perform differently in distinct parameter regimes.

3. Extended nanosystems: the dual-fermion formalism

In this section we review the dual-fermion formalism. We introduce it in a formulation suitable for a realistic treatment of nanosystems. A more detailed introduction can be found in [20, 21].

Let us be specific and consider a system consisting of a one-dimensional chain or two-dimensional overlayer of multiorbital atoms on top of a metallic substrate. For notational convenience, we introduce spinors $\mathbf{c}_{\omega\mathbf{k}\sigma} = (\ldots, c_{\omega\mathbf{k}\sigma m},\ldots)$, $\mathbf{c}^*_{\omega\mathbf{k}\sigma} = (\ldots, c^*_{\omega\mathbf{k}\sigma m},\ldots)$. In this notation, for example, the Green functions are matrices in orbital space. The system can be modeled by means of the imaginary time action

$$S[\mathbf{c}^*,\mathbf{c}] = -\sum_{\omega\mathbf{k}\sigma}\mathbf{c}^*_{\omega\mathbf{k}\sigma}\left((\mathrm{i}\omega+\mu)\mathbf{1}-h_{\mathbf{k}\sigma}\right)\mathbf{c}_{\omega\mathbf{k}\sigma} + \sum_i\mathbf{c}^*_{\omega i\sigma}(\Delta^{(s)}_{\omega\sigma})\mathbf{c}_{\omega i\sigma} + \sum_i H_{\rm int}[\mathbf{c}_i^*,\mathbf{c}_i], \quad (17)$$

where $\omega_n = (2n+1)\pi/\beta, n = 0,\pm1,\ldots$ are the Matsubara frequencies, β is the inverse temperature, μ is the chemical potential, $\sigma = \uparrow,\downarrow$ labels the spin projection and $\mathbf{c}^*,\mathbf{c}$ are Grassmann variables which embody the fermionic degrees of freedom in the path integral representation. The index i labels the lattice sites and the $\mathbf{k}$ vectors are quasimomenta. Here $h_{\mathbf{k}\sigma}$ is the dispersion of the Hamiltonian describing the noninteracting freestanding chain. The (generally frequency-dependent) matrix $\Delta^{(s)}$ accounts for the hybridization with the metallic or insulating substrate. The locality of $H_{\rm int}$ is the only requirement for the otherwise arbitrary interaction. A realistic description of the atomic degrees of freedom is provided by the general Coulomb interaction

$$H_{\rm int}[\mathbf{c}_i^*,\mathbf{c}_i] = \tfrac{1}{4}\int_0^\beta \mathrm{d}\tau\, U_{1234}c^*_{i1}(\tau)c^*_{i2}(\tau)c_{i4}(\tau)c_{i3}(\tau), \quad (18)$$

where U is the general antisymmetrized Coulomb vertex and, for example, $1\equiv\{m_1\sigma_1\}$ comprehends orbital and spin degrees of freedom and summation over these states is implied.

Owing to the fact that efficient solvers exist to solve the impurity problem, it seems natural to divide the action equation (17) into a numerically exactly solvable local impurity part and an itinerant bilinear term:

$$S[\mathbf{c}^*,\mathbf{c}] = \sum_i S_{\rm imp}[\mathbf{c}^*_{\omega i\sigma},\mathbf{c}_{\omega i\sigma}] - \sum_{\omega\mathbf{k}\sigma}\mathbf{c}^*_{\omega\mathbf{k}\sigma}\left(\Delta_{\omega\sigma}-h_{\mathbf{k}\sigma}\right)\mathbf{c}_{\omega\mathbf{k}\sigma}. \quad (19)$$

Here the additional hybridization Δ is introduced to describe the local environment of an atom created by the atoms on all other sites in the chain. The impurity problem, which can be solved by the methods presented in the previous section, is now

$$S_{\rm imp}[\mathbf{c}^*,\mathbf{c}] = -\sum_{\omega\sigma}\mathbf{c}^*_{\omega\sigma}\left((\mathrm{i}\omega+\mu)\mathbf{1}-\tilde{\Delta}_{\omega\sigma}\right)\mathbf{c}_{\omega\sigma} + H_{\rm int}[\mathbf{c}^*,\mathbf{c}], \quad (20)$$

where $\tilde{\Delta}_{\omega\sigma} = \Delta_{\omega\sigma} + \Delta^{(s)}_{\omega\sigma}$. Now dual fermions are introduced in the path integral via the Gaussian identity

$$\int\exp(-\mathbf{f}^*[g^{-1}_{\omega\sigma}(\Delta_{\omega\sigma}-h_{\mathbf{k}\sigma})^{-1}g^{-1}_{\omega\sigma}]\mathbf{f}-\mathbf{f}^*g^{-1}_{\omega\sigma}\mathbf{c}-\mathbf{c}^*g^{-1}_{\omega\sigma}\mathbf{f}) \times\mathcal{D}[\mathbf{f}^*,\mathbf{f}] = \det(g^{-1}_{\omega\sigma}\left(\Delta_{\omega\sigma}-h_{\mathbf{k}\sigma}\right)^{-1}g^{-1}_{\omega\sigma}) \times\exp\left(\mathbf{c}^*\left(\Delta_{\omega\sigma}-h_{\mathbf{k}\sigma}\right)\mathbf{c}\right). \quad (21)$$

The variables $\mathbf{f}, \mathbf{f}^*$ represent the auxiliary (dual) degrees of freedom. The original action becomes

$$S[\mathbf{c}^*, \mathbf{c}, \mathbf{f}^*, \mathbf{f}] = \sum_i S_{\mathrm{site},i}[\mathbf{c}^*, \mathbf{c}, \mathbf{f}^*, \mathbf{f}] + \sum_{\omega \mathbf{k} \sigma} \left[\mathbf{f}^*_{\omega \mathbf{k}\sigma} g^{-1}_{\omega\sigma} \left(\Delta_{\omega\sigma} - h_{\mathbf{k}\sigma}\right)^{-1} g^{-1}_{\omega\sigma} \mathbf{f}_{\omega \mathbf{k}\sigma}\right] \tag{22}$$

where the local part of the action S_{imp} is the only term that retains degrees of freedom of the original fermions:

$$S_{\mathrm{site},i} = S_{\mathrm{imp}}[\mathbf{c}^*_i, \mathbf{c}_i] + \mathbf{f}^*_{\omega i\sigma} g^{-1}_{\omega\sigma} \mathbf{c}_{\omega i\sigma} + \mathbf{c}^*_{\omega i\sigma} g^{-1}_{\omega\sigma} \mathbf{f}_{\omega i\sigma}. \tag{23}$$

Due to the locality of $g_{\omega\sigma}$ (the impurity Green function) the summation over all states labeled by $\mathbf{k}$ in the second term could be replaced by the equivalent summation over all sites. The fact that S_{site} decomposes into a sum of local terms is crucial and allows us to integrate out the lattice fermions for each site separately:

$$\int \exp\left(-S_{\mathrm{site}}[\mathbf{c}^*_i, \mathbf{c}_i, \mathbf{f}^*_i, \mathbf{f}_i]\right) \mathcal{D}[\mathbf{c}^*_i, \mathbf{c}_i] = \mathcal{Z}_{\mathrm{imp}} \mathrm{e}^{-\left(\sum_{\omega\sigma} \mathbf{f}^*_{\omega i\sigma} g^{-1}_{\omega\sigma} \mathbf{f}_{\omega i\sigma} + V_i[\mathbf{f}^*_i, \mathbf{f}_i]\right)}, \tag{24}$$

where $\mathcal{Z}_{\mathrm{imp}}$ is the partition function of the impurity. Formally this can be done up to all orders and, in this sense, the transformation to the dual fermions is exact. The above equation may be viewed as the defining equation for the dual potential $V[\mathbf{f}^*, \mathbf{f}]$. After expanding both sides of equation (24), integrating out on the left-hand side corresponds to averaging over the impurity degrees of freedom. Equating the resulting expressions by order, one finds that the dual potential in the lowest-order approximation is given by

$$V[\mathbf{f}^*, \mathbf{f}] = \tfrac{1}{4} \sum_i \gamma^{(4)}_{1234} \mathbf{f}^*_{i1} \mathbf{f}^*_{i2} \mathbf{f}_{i4} \mathbf{f}_{i3} + \cdots, \tag{25}$$

where

$$\gamma^{(4)}_{1234} = g^{-1}_{11'} g^{-1}_{22'} \left[\chi^{\mathrm{imp}}_{1'2'3'4'} - \chi^{\mathrm{imp},0}_{1'2'3'4'}\right] g^{-1}_{3'3} g^{-1}_{4'4}, \qquad \chi^{\mathrm{imp},0}_{1234} = g_{14} g_{23} - g_{13} g_{24} \tag{26}$$

is the exact four-point reducible local vertex, constructed from the two-particle Green function of the impurity. While in principle higher-order momenta of the impurity appear in V, we will restrict ourselves to the lowest-order approximation in the following.

After integrating out, the action depends on dual variables only and can be written as

$$S_{\mathrm{d}}[\mathbf{f}^*, \mathbf{f}] = -\sum_{\omega \mathbf{k}\sigma} \mathbf{f}^*_{\omega \mathbf{k}\sigma} (G^{\mathrm{d},0}_{\omega \mathbf{k}\sigma})^{-1} \mathbf{f}_{\omega \mathbf{k}\sigma} + \sum_i V[\mathbf{f}^*_i, \mathbf{f}_i], \tag{27}$$

where the bare dual Green function is given by

$$G^{\mathrm{d},0}_{\omega \mathbf{k}\sigma} = -g_{\omega\sigma} \left[g_{\omega\sigma} + \left(\Delta_{\omega\sigma} - h_{\mathbf{k}\sigma}\right)^{-1}\right]^{-1} g_{\omega\sigma}. \tag{28}$$

Up to now we have only reformulated the problem. The solution can be obtained in terms of the self-energy by performing a regular diagrammatic series expansion in the potential V. In practice, the series for the dual potential and the perturbation series need to be terminated at some point.

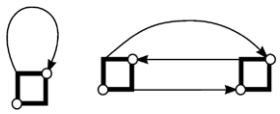

Figure 2. The first two lowest-order diagrams for the dual self-energy Σ^{d}.

The two lowest-order (skeleton) diagrams of this expansion are shown in figure 2. The first diagram is local, while the second brings in a non-local correction to the self-energy. As we shall see in the next section, already this seemingly crude approximation delivers very reasonable results. Since the decomposition of the original problem into the impurity and the itinerant parts is obviously independent of the hybridization function Δ, this function has not been specified so far. We construct a self-consistency condition for this quantity by requiring that the lowest-order local correction, i.e. the first diagram in figure 2, be zero. In this case we recover exactly the self-consistency condition of the DMFT. Our expansion can thus be seen as a perturbation expansion around the DMFT. As is well known, the DMFT becomes exact in the limit of infinite coordination number. Hence the DMFT hybridization likely delivers a poor description of the local environment of an atom, in particular for the low-dimensional structures in nanosystems. Indeed we shall see in the next section that the renormalization of the hybridization according to the self-consistency condition is crucial for the scheme and strongly improves the result for the 1D chain.

It should be pointed out that the above series expansion is an expansion for the dual fermions and does not correspond to the solution of the original problem. However, the fact that we have introduced the dual fermions via an exact transformation, equation (21), allows us to establish an exact relation between original and dual quantities (the latter labeled by 'd'), like the Green function:

$$G_{\omega \mathbf{k}\sigma} = \left(\Delta_{\omega\sigma} - h_\sigma(\mathbf{k})\right)^{-1} g^{-1}_{\omega\sigma} G^{\mathrm{d}}_{\omega \mathbf{k}\sigma} g^{-1}_{\omega\sigma} \left(\Delta_{\omega\sigma} - h_\sigma(\mathbf{k})\right)^{-1} + \left(\Delta_{\omega\sigma} - h_\sigma(\mathbf{k})\right)^{-1}. \tag{29}$$

A corresponding relation is also available for the two-particle Green function. For clarity, we omit indices and write it symbolically as

$$\tilde{\chi} = \left[(\Delta - h)^{-1} g^{-1}\right] \left[(\Delta - h)^{-1} g^{-1}\right] (\tilde{\chi}^{\mathrm{d}}) \times \left[g^{-1} (\Delta - h)^{-1}\right] \left[g^{-1} (\Delta - h)^{-1}\right] \tag{30}$$

where the tilde denotes the nontrivial part, which diagrammatically corresponds to the vertex part with four Green function legs attached. The terms in square brackets only contain single-particle functions. Two-particle excitations are hence the same for dual and lattice fermions.

4. Selected results

In this section we illustrate these concepts by results for a freestanding chain at half-filling described by the one-dimensional (1D) Hubbard Hamiltonian:

$$-t \sum_{i\sigma} \left(c^*_{\sigma\, i+1} c_{\sigma\, i} + c^*_{\sigma\, i-1} c_{\sigma\, i}\right) + U \sum_i n_{\uparrow\, i} n_{\downarrow\, i}. \tag{31}$$

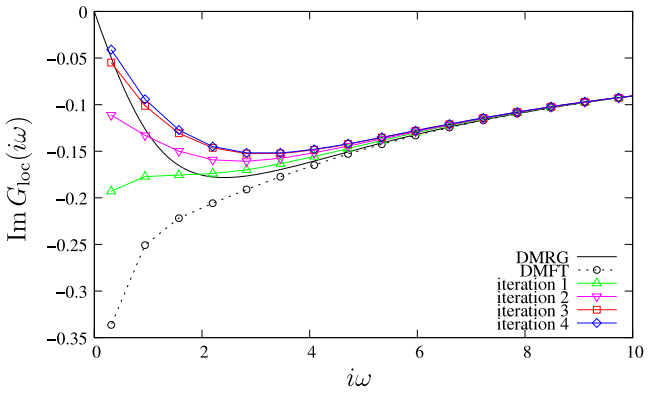

Figure 3. Imaginary part of the local Matsubara Green function for the 1D Hubbard model with $U/t = 6$ and $T/t = 0.1$. The results from various dual-fermion iterations are compared to the zero temperature DMRG Green function and the DMFT result.

The bare dispersion is given by $h_k = -2t\cos(ka)$. Figure 3 shows the local part of the Green function as a function of Matsubara frequencies. We compare the results from the dual-fermion calculations to the one of an essentially exact density matrix renormalization group calculation [24, 25] (DMRG) at $T = 0$. It is clearly seen that the DMFT result in this figure is qualitatively incorrect as it predicts the system to be metallic. In the dual-fermion calculations the tendency to an insulator can be seen already for the first dual-fermion iteration: the Green function at the lowest Matsubara frequency bends up as the hybridization Δ is renormalized during successive iterations. The final result correctly shows insulating behavior. It has been shown that in a cluster dual-fermion calculation the result is substantially improved [26]. However, the single-site approach is particularly appealing since it provides a translationally invariant solution.

We note that, while there is no multiorbital formulation of the DMRG, our approach offers a qualitative description of 1D multiorbital systems. The present results may be further improved by calculating the dual self-energy using more diagrams, e.g. by a ladder diagram summation. This work is in progress now and opens a way towards a realistic and quantitative description of adatom chains on surfaces.

In order to address the issue of long-range order, we have generalized our approach to facilitate the calculation of the two-particle Green functions. This allows us to determine magnetic instabilities. The dual two-particle Green function is obtained from the two-particle vertex, which we find by means of a Bethe–Salpeter equation depicted diagrammatically in figure 4. The exact relation, which allows us to obtain the two-particle Green function of the original fermions, was given in equation (30). Figure 5 shows the dual spin–spin susceptibility as obtained from the diagram in figure 4 as a function of temperature. The results were obtained for the 2D Hubbard model at half-filling, for $U/t = 4$ [21]. For lattice and dual fermions the susceptibilities diverge in the $\mathbf{q} = (\pi, \pi)$ channel corresponding to the antiferromagnetic instability.

In the inset of this figure we show the numerical illustration of the statement that two-particle excitations and corresponding instabilities are the same for dual and lattice

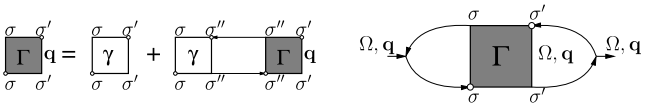

Figure 4. Left: the Bethe–Salpeter equation for the dual vertex in the $Sz = 0$ particle–hole channel. Right: diagram for the dual susceptibility $\tilde{\chi}^{\rm d}_{zz}$.

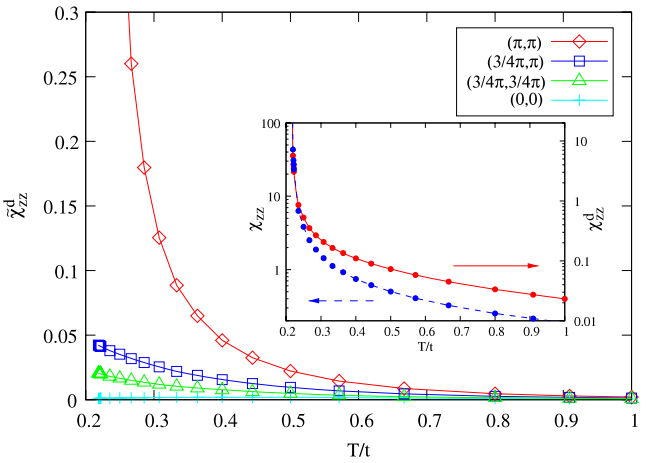

Figure 5. Nontrivial part of the dual susceptibility $\tilde{\chi}^{\rm d}_{zz}$ calculated from the diagram in figure 4 for different values of the transferred momentum $\mathbf{q}$. The instability occurs in the $\mathbf{q} = (\pi, \pi)$ channel. Inset: comparison between the dual susceptibility $\chi^{\rm d}_{zz} = \chi^{\rm d0}_{zz} + \tilde{\chi}^{\rm d}_{zz}$ and the lattice susceptibility χ_{zz} for $\mathbf{q} = (\pi, \pi)$. The instability is the same for dual and lattice fermions. Note the different scales.

fermions. Although the susceptibilities are different in magnitude, they diverge at the same temperature.

5. Concluding remarks

We have discussed recent developments in the field of quantum Monte Carlo solvers for the numerically exact solution of the multiorbital impurity that may be used to describe adatoms on surfaces. It was shown how two-particle correlation functions can be measured in imaginary time. Analytical continuation to the real axis provides information on two-particle excitations. We have introduced the dual-fermion approach in a formulation that allows us to incorporate the material aspect into calculations of extended low-dimensional nanosystems, such as monatomic chains on a substrate with arbitrary density of states. It was shown that already the lowest-order approximation gives very promising results even for low-dimensional systems. We have further demonstrated that susceptibilities can be calculated in this approach, which allows us to address the problem of long-range order in nanosystems.

Acknowledgment

Financial support from DFG Grant No. SFB 668 (Germany) is gratefully acknowledged.

References

[1] Ternes M, Lutz C P, Hirjibehedin C F, Giessibl F J and Heinrich A J 2008 The force needed to move an atom on a surface *Science* **319** 1066–9

[2] Ding H F, Stepanyuk V S, Ignatiev P A, Negulyaev N N, Niebergall L, Wasniowska M, Gao C L, Bruno P and Kirschner J 2007 Self-organized long-period adatom strings on stepped metal surfaces: scanning tunneling microscopy, *ab initio* calculations, and kinetic Monte Carlo simulations *Phys. Rev.* B **76** 033409

[3] Hirjibehedin C F, Lutz C P and Heinrich A J 2006 Spin coupling in engineered atomic structures *Science* **312** 1021–4

[4] Meier F, Zhou L, Wiebe J and Wiesendanger R 2008 Revealing magnetic interactions from single-atom magnetization curves *Science* **320** 82–6

[5] Kolesnychenko O Yu, de Kort R, Katsnelson M I, Lichtenstein A I and Kempen H 2002 Real-space imaging of an orbital Kondo resonance on the cr(001) surface *Nature* **415** 507–9

[6] Chen W, Jamneala T, Madhavan V and Crommie M F 1999 Disappearance of the Kondo resonance for atomically fabricated cobalt dimers *Phys. Rev.* B **60** R8529–32

[7] Jamneala T, Madhavan V and Crommie M F 2001 Kondo response of a single antiferromagnetic chromium trimer *Phys. Rev. Lett.* **87** 256804

[8] Savkin V V, Rubtsov A N, Katsnelson M I and Lichtenstein A I 2005 Correlated adatom trimer on a metal surface: a continuous-time quantum Monte Carlo study *Phys. Rev. Lett.* **94** 026402

[9] Lagoute J, Liu X and Fölsch S 2005 Link between adatom resonances and the Cu(111) Shockley surface state *Phys. Rev. Lett.* **95** 136801

[10] Pratzer M, Elmers H J, Bode M, Pietzsch O, Kubetzka A and Wiesendanger R 2001 Atomic-scale magnetic domain walls in quasi-one-dimensional Fe nanostripes *Phys. Rev. Lett.* **87** 127201

[11] Lagoute J, Nacci C and Fölsch S 2007 Doping of monatomic Cu chains with single Co atoms *Phys. Rev. Lett.* **98** 146804

[12] Mermin N D and Wagner H 1966 Absence of ferromagnetism or antiferromagnetism in one- or two-dimensional isotropic Heisenberg models *Phys. Rev. Lett.* **17** 1133–6

[13] Gambardella P, Dallmeyer A, Maiti K, Malagoli M C, Eberhardt W, Kern K and Carbone C 2002 Ferromagnetism in one-dimensional monatomic metal chains *Nature* **416** 301–4

[14] Brovko O O, Ignatiev P A, Stepanyuk V S and Bruno P 2008 Tailoring exchange interactions in engineered nanostructures: an *ab initio* study *Phys. Rev. Lett.* **101** 036809

[15] Kotliar G, Savrasov S Y, Haule K, Oudovenko V S, Parcollet O and Marianetti C A 2006 Electronic structure calculations with dynamical mean-field theory *Rev. Mod. Phys.* **78** 865

[16] Hirsch J E and Fye R M 1986 Monte Carlo method for magnetic impurities in metals *Phys. Rev. Lett.* **56** 2521–4

[17] Rubtsov A N, Savkin V V and Lichtenstein A I 2005 Continuous-time quantum Monte Carlo method for fermions *Phys. Rev.* B **72** 035122

[18] Werner P, Comanac A, de' Medici L, Troyer M and Millis A J 2006 Continuous-time solver for quantum impurity models *Phys. Rev. Lett.* **97** 076405

[19] Haule K 2007 Quantum Monte Carlo impurity solver for cluster dynamical mean-field theory and electronic structure calculations with adjustable cluster base *Phys. Rev.* B **75** 155113

[20] Rubtsov A N, Katsnelson M I and Lichtenstein A I 2008 Dual fermion approach to nonlocal correlations in the Hubbard model *Phys. Rev.* B **77** 033101

[21] Brener S, Hafermann H, Rubtsov A N, Katsnelson M I and Lichtenstein A I 2008 Dual fermion approach to susceptibility of correlated lattice fermions *Phys. Rev.* B **77** 195105

[22] Mishchenko A S, Prokof'ev N V, Sakamoto A and Svistunov B V 2000 Diagrammatic quantum Monte Carlo study of the Fröhlich polaron *Phys. Rev.* B **62** 6317–36

[23] Hafermann H, Katsnelson M I and Lichtenstein A I 2008 Metal–insulator transition by suppression of spin fluctuations *Europhys. Lett.* submitted

[24] White S R 1992 Density matrix formulation for quantum renormalization groups *Phys. Rev. Lett.* **69** 2863–6

[25] Jeckelmann E 2002 Ground-state phase diagram of a half-filled one-dimensional extended Hubbard model *Phys. Rev. Lett.* **89** 236401

[26] Hafermann H, Brener S, Rubtsov A N, Katsnelson M I and Lichtenstein A I 2007 Cluster dual fermion approach to nonlocal correlations *JETP Lett.* **86** 677